Evaluation of Landfalling Atmospheric Rivers along the U.S. West Coast in Reanalysis Data Sets

Darren L. Jackson and Mimi Hughes

Cooperative Institute for Research in Environmental Sciences and NOAA Earth System Research Laboratory, Boulder, Colorado

Gary A. Wick

NOAA Earth System Research Laboratory, Boulder, Colorado

KEY POINTS

- Satellite data are used to assess atmospheric river landfall events in four reanalysis data sets
- Overall landfall detections for three reanalysis data sets were within 5% of satellite data result

ABSTRACT

An intercomparison of landfalling atmospheric rivers (ARs) between four reanalysis data sets using one satellite-derived AR detection method as a metric to characterize landfalling atmospheric rivers (ARs) along the U.S. West Coast is performed over 15 cool seasons (October – March) during the period from water years 1998 to 2012. The four reanalysis data sets analyzed in this study are the Climate System Forecast Reanalysis (CFSR), Modern-Era Retrospective Analysis for Research and Applications (MERRA), ERA-Interim (ERA-I), and the Twentieth Century Reanalysis version 2 (20CR) data set. The Atmospheric River Detection Tool (ARDT) is used to identify AR features in the total vertically integrated water vapor (IWV) data of the reanalysis data and validation of the reanalysis AR data are compared with AR data derived from satellite IWV observations. The AR landfall data from reanalysis were generally found to be in good agreement with satellite observations. Reanalysis data with less (CFSR) or no assimilation (20CR) of the satellite data used in this study had greater bias with AR characteristics such as IWV, width, and landfall location. 20CR ensemble data was found to better characterize the AR landfall characteristics than the 20CR ensemble mean although all 20CR data underestimated AR landfalls particularly in the southern section of the U.S West Coast. Overall AR landfall detections for the 15-year cool season period were within 5% of the satellite for the CFSR, MERRA, and ERA-I data.

1. INTRODUCTION

Atmospheric rivers (ARs) are long and narrow water vapor features of enhanced water vapor flux found in the lower troposphere that are responsible for transporting approximately 90% of water vapor from the tropics to the mid-latitudes [Zhu and Newell, 1998]. ARs are responsible for up to 50% of U.S. West Coast annual rainfall [Dettinger et al., 2011], and they are the primary mechanism for generating extreme precipitation and major flooding in this region [Ralph and Dettinger, 2012]. Evaluating sub-seasonal, seasonal, and interannual variability of AR landfalls for the U.S. West Coast with reanalysis data sets is attractive because these data have better temporal sampling than polar orbiting satellite observations and can extend well before the satellite era as is the case for the Twentieth Century Reanalysis (20CR) [Compo et al., 2011] and the National Center for Environmental Prediction (NCEP)/ National Center for Atmospheric Research (NCAR) reanalysis data sets. This study evaluates AR features in four different reanalysis data sets and compares them to an established satellite AR data set [Wick et al., 2013a] over 15 cool seasons (October – March) for water years 1998 through 2012.

Numerous AR studies characterizing the structure and frequency of AR events using satellite data have been conducted over the past 10 years. Ralph et al. [2004] provided the framework for using satellite-derived total vertically integrated water vapor (IWV) in order to characterize U.S. West Coast ARs and established water vapor plumes with IWV > 2 cm as a threshold and width and length scales of < 1000 km and > 2000 km, respectively, for AR identification in this region. Neiman et al. [2008] developed the first climatology of AR landfalling events on the West Coast from 1997 to 2005 by visually inspecting satellite IWV imagery. However, developing climatologies from visual inspection becomes burdensome when analyzing long term data sets or determining AR characteristics objectively from real-time evaluation of satellite or model IWV fields. Therefore, Wick et al. [2013a] developed an AR detection tool (ARDT) using the characteristics established in these previous studies to identify AR features in satellite IWV fields derived from Defense Meteorological Satellite Program (DMSP) Special Sensor Microwave/Imager (SSM/I) and Special Sensor Microwave Imager/Sounder (SSMIS) observations. The ARDT successfully identified ARs along the U.S. West Coast with a probability of detection of 98.5% and false detection rate of < 5% when compared with the visual AR climatology in Neiman et al. [2008]. An additional study by Wick et al. [2013b] used the ARDT to evaluate AR forecasts from model IWV data for five numerical weather prediction models and found the occurrence of ARs to be well forecasted with probability of AR detection greater than 84% and false alarms less than 12 % at a 10-day lead time.

Reanalysis data sets have been used to study ARs typically in the context of examining impacts on extreme precipitation and flooding events. Studies using NCEP/NCAR reanalysis [Neiman et al., 2008, Ralph et al., 2011], North American Regional Reanalysis data set [Neiman et al., 2011], ERA-I [Runtz et al., 2014; Lavers and Villarini, 2013], MERRA [Ryoo et al., 2013; Payne and Magnusdottir, 2014], and 20CR [Lavers et al., 2012] have identified ARs in these data sets and relationships to extreme precipitation and flooding. Alternative methods for detecting ARs using an IVT thresholding method [Rutz et al., 2014] or percentiles of the IVT distribution [Lavers et al., 2012, Payne and Magnusdottir, 2014] have been developed for reanalysis data sets. Lavers et al. [2012] featured five reanalysis products (CFSR, MERRA, ERA-I, 20CR, and NCEP) in their study to determine linkages with British winter floods with ARs. They conducted a 31-year study for this region and found good agreement for AR occurrences between the five reanalysis products. However, no comprehensive study has been done to assess the skill of AR landfalls along the U.S. West Coast among these various reanalysis data sets against satellite observations.

In this study, the ARDT is applied to IWV data from four reanalysis data sets and evaluated against the AR statistics derived from satellite data for the U.S. West Coast region for the cool-season portion of the water years from 1998 to 2012. While IVT is a more direct parameter for identifying water vapor flux associated with AR signatures, satellite retrievals of IWV data are used here because satellites are not capable of discerning vertical wind profiles required to derive IVT. The evaluation is primarily focused on comparing AR landfall similarities and differences between the reanalysis products. Should the evaluation of ARs derived from reanalysis data against satellite data prove that reanalysis data can reliably produce AR features, then greater confidence can be subscribed to the AR climatologies developed from these products particularly during the satellite era.

This paper will describe the data sets used for this study in Section 2. The methodology of AR identification is provided in Section 3 along with the issues of AR identification from data sets of various spatial resolutions. Section 4 evaluates AR landfalls among the various reanalysis products and how they compare with the AR landfall data from satellite observations. Conclusions are then provided in Section 5.

2. DATA

2.1 Satellite data

IWV data derived from satellite observations were used to develop the AR validation data set for the reanalysis data products. SSM/I and SSMIS observations from the Defense Meteorological Satellite Program (DMSP) polar-orbiting satellites were used in this study. Twice daily 0.5^{o} x 0.5^{o} gridded data were generated utilizing all available sensors from 1997 through 2012 for time periods 0000–1159 UTC and 1200–2359 UTC, and it is these satellite data that define the time period for this study. Combining data from multiple sensors eliminated most gaps in coverage; however, gaps were identified and accounted for in the analysis as will be discussed in section 4.1. Retrievals of satellite IWV were generated using the Wentz [1995] statistical algorithm which has been used extensively in previous AR studies [Wick et al., 2013b, Neiman et al., 2013].

2.2 Reanalysis data

Reanalyses are multiyear gridded data that represent the state of the atmosphere using a constant model and a data assimilation system. Four reanalysis data sets were used in this study: The NCEP Climate System Forecast Reanalysis (CFSR) [Saha et al., 2010], the NASA Modern-Era Retrospective Analysis for Research and Applications (MERRA) [Rienecker et al., 2011], the ERA-Interim (ERA-I) [Dee et al., 2011], and the Twentieth Century Reanalysis version 2

(20CR) data set [Compo et al., 2011]. Table 1 provides the temporal and spatial characteristics from each of the data sets. All four data sets have 6-hourly product output but only 0000 and 1200 UTC times were used in this study since they best correspond in time with the satellite observations. All four data sets have a time range coincident with the satellite time period used in this study.

Different levels of assimilating the satellite observations used in this study were incorporated for the four reanalysis data sets. CFSR, MERRA, and ERA-I assimilated SSM/I data (among many other observations and products), although the specifics of the SSM/I assimilation varied: CFSR assimilated only the retrievals of the SSM/I-derived surface winds, MERRA assimilated SSM/I radiances, retrievals of rain rate and wind speed, and ERA-I assimilated both SSM/I and SSMIS radiances. The 20CR only assimilated sea-surface temperature and sea ice concentration fields from the Hadley Centre Sea Ice and SST dataset (HadISST) [Rayner et al., 2003] and surface pressure provided through the International Surface Pressure Databank (ISPD).

3. METHOD

The ARDT is an automated objective tool for identifying and characterizing ARs using IWV fields [Wick et al., 2013a]. We applied the ARDT to SSM/I and SSMIS satellite retrievals of IWV and to the four reanalysis IWV fields over 15 cool seasons (October–March) for water years 1998 to 2012. The ARs were identified using the ARDT over the domain from 15°N–55°N and 160°W–110°W which covers the entire western coastline of the continental United States.

The ARDT was applied to twice daily SSM/I and SSMIS satellite observations which were composited for the 0000–1159 UTC and 1200–2359 UTC time periods. Since most of the DMSP satellite observations in the northeast Pacific region occur in the 0100–0400 UTC and 1300–1600 UTC time period, the ARDT was applied to only the 0000 and 1200 UTC reanalysis data fields. AR satellite data are used primarily as a validation dataset rather than a climatological data set in this study.

The ARDT identifies ARs using a skeletonization method [Wick et al., 2013a] to locate potential core points along IWV features determined by thresholds ≥ 2 cm. Wick et al. [2013a] provides details of the AR identification method. Key outputs from the ARDT for each IWV field are the number of identified ARs and their locations. Locations are provided as a list of axis points determined by the ARDT. At each axis point, other key parameters provided are the (1) IWV core value at the axis location, (2) the width of the AR at pre-defined IWV thresholds of 2.0, 2.67, 3.0, 3.33, 3.67, and 4.0 cm, (3) the AR directional angle, and (4) landfall latitude.

AR landfall characteristics of these key parameters from the reanalysis and satellite products are examined in this study. All landfall statistics were averaged using all available AR data from 100–200 km from the coast and conditioned on the presence of an observed satellite AR. Since ARs typically propagate westward and have a minimum width of ~250 km, these statistics were considered representative of ARs associated with a landfall. The IWV core value is the IWV at the axis location which is defined as the center point along the shortest transect crossing the AR at that location. AR width values are defined at various IWV thresholds (2.0, 2.33, and 2.67 cm).

Here we use the minimum width for these thresholds to define the average since slight variations in IWV values between the reanalysis products could bias widths for any given threshold. Landfall latitude is the average latitude location defined by the set of AR axis locations within the 100–200 km coastal region. Information within 100 km of the coast was not included since microwave satellite observations risk having sidelobe contamination due to high land emissivity. Figure 1 shows an example of the domain used to identify ARs in this study and an AR signature in the satellite and reanalyses IWV fields that occurred March 27, 2005. This AR event [Ralph et al., 2011] induced orographically-enhanced precipitation that was responsible for high stream flows and ended a drought in the Pacific Northwest. Over the AR axis locations (grey dots of Figure 1), a flag is set indicating whether the axis location is near the coast. It is from application of the ARDT to IWV fields shown in Figure 1 that AR landfall characteristics are developed for this study.

Gaps in satellite coverage, due to missing satellite orbits or gaps between orbits that prevented the ARDT from detecting AR events were accounted for in the reanalysis products when directly comparing AR landfall events between reanalysis and satellite observations. The number of grid cells with missing satellite IWV data that have a minimum distance from the North American coast line between 100 and 2000 km were accumulated for each 12-hour period (0000–1159 and 1200–2359 UTC) for the 15 winter seasons. Missing data in other regions of the domain were not identified as gaps because the missing data were sufficiently far from coast line to not impact identifying an AR landfall. A significant gap was identified as having > 1% of the grid cells missing in the 100 to 2000 km region near the coast line for each 12-hour period (hereafter referred to as fields). From a total of 5468 fields, 4404 fields were deemed viable for input to

ARDT and 1064 were excluded. Of the 1064 excluded fields, 1015 fields were found to have significant gaps and 49 fields had no valid data in the entire domain. Among the 4404 fields deemed viable, 70 fields had missing data in 100–2000 km region near the U.S. West Coastline but did not exceed 1%. And finally, 22 of the 4404 fields had an identified AR landfall despite exceeding the 1% significant gap threshold. These fields were used and considered valid since missing data did not negatively impact ARDT from identifying an AR landfall.

A common 0.5^o spatial resolution was selected for all reanalysis and satellite data used as input to the ARDT. 20CR, MERRA, and ERA-I were bilinearly interpolated to 0.5^o spatial resolution while CFSR required no interpolation since it was already at this resolution. Increasing the resolution of the lower resolution data sets to the highest resolution data set was desirable since subsampling to a lower resolution grid would result in losing information in the IWV imagery that would adversely impact the ability of the ARDT to identify an AR. A 7x7 median filter was applied to the native 0.25^o satellite grid data, prior to subsampling the satellite to 0.5^o grid data, in order to reduce measurement noise and fill small gaps that sometimes impacts identification of continuous features in the IWV imagery [Wick et al., 2013a]. A smaller 3x3 median filter was applied to the 0.5^o CFSR, MERRA, and ERA-I reanalysis data sets due to less noise in these fields, and no filter was applied to the 20CR data set because minimal impact was found using a filter due to its lower spatial resolution. Reanalysis data were masked over land to simulate the satellite IWV data which are not available over land and to prevent AR detections in reanalysis data that would extend over land.

Because the ARDT relies on specific IWV thresholds to identify ARs, bias in IWV between the various data sets was computed and IWV bias adjustments were applied to minimize AR identification differences between the data sets. The bias between satellite and each reanalysis data set was determined by computing a mean bias over the whole northeastern Pacific domain [Wick et al., 2013b]. The cool season of water year 2005 was chosen for this correction since it centered the study period and only small interannual variations in bias between reanalysis and satellite data were found. The largest bias correction was 0.12 cm for the 20CR data.

4. AR LANDFALL ANALYSIS

Characteristics of the U.S. West Coast AR landfalls are first examined through application of the ARDT to the satellite observations. The four reanalysis data sets are then compared with the AR statistics derived from satellite observations to compare differences with observations and among the different reanalysis products.

4.1 Satellite AR validation data

The first step in the analysis of 15 years of AR detection data was to examine the satellite validation data for AR locations and landfalls during the cool season for water years 1998–2012. A frequency map of AR axis locations from the satellite IWV observations over the 15-year period during the cool season is shown in Figure 2. Highest values occur in the western side of the domain north of Hawaii and extend to the northeast toward northwest coast of the United States. This southwest to northeast orientation remains throughout the six month cool season but shifts southward from October to March (not shown). The southward shift is related to the seasonal reduction in the IWV background state during the cool season. Neiman et al. [2008] also found the cool season ARs in this region to have this preferential orientation.

Since the focus of this paper is to examine AR landfalls along the United States West Coast, Figure 3a shows the frequency and percentage of AR landfalls as determined from the satellite data for each cool season during the 15-year period. The AR frequency is the total number of AR landfall detections based on twice daily IWV fields over the cool season which has a maximum of 362 analyzed IWV fields per cool season (during 182 non-leap year days). The AR landfall percentage is the number of fields with ARs divided by the total number fields (but excluding fields with data gaps). Note that frequency statistics do not measure the number of AR days as in previous studies, and do not account for AR evolution over consecutive time steps. Figure 3b shows the number of fields removed each year due to gaps in satellite coverage (Section 3). The decrease in gap occurrences starting in 2008 is related to the transition from SSM/I to SSMIS observations which increases the swath width ~300 km and reduces gaps between satellite orbits. The frequency time series in Figure 3a shows significant variability from ~75 to ~135 landfall detections for a given cool season. Gaps in satellite coverage explain some of the variability and the increase in AR frequency in the later part of the period; however, the percentage of AR detections available each year still shows an annual variation from 27 to 43% from 2009 to 2011 when satellite coverage was relatively high. Seasonal and interannual variations in AR landfalls due to natural phenomena, such as the Madden-Julian Oscillation

(MJO) and the El Niño/Southern Oscillation (ENSO), also likely impact AR landfall frequency but quantifying their effects are beyond the scope of this study. The percentage of days detected to have ARs each cool season (not shown) ranges from 30–50% which is a little higher than shown in Figure 3a since only one detection per day is required to meet this criterion.

The frequency and percentage of AR detections over the 15-year period as a function of month is shown in Figure 4. AR landfall frequency and percentage maximum occurs in October with 47% of the satellite IWV images showing a U.S. West Coast AR landfall during this month. AR frequency is highest in October due to the high number of northern U.S. West Coast AR landfalls during the summer and fall seasons [Neiman et al., 2008] and due to the higher background water vapor state in the early period of the cool season. Both AR landfall percentage and frequency decrease through the cool season with only a 22% AR landfall percentage in February followed by an increase in March AR landfalls. A reduced number of detected AR landfalls in January and February may also be affected by a lower IWV background where AR-like features fall below the 2 cm threshold. This monthly climatology agrees well with the manually-identified climatology shown in Neiman et al. [2008] even though they use a different AR landfall statistic (AR days) and base time period for their study.

The number of AR landfall detections in this study exceeds those shown in previous papers [Neiman et al., 2008; Wick et al., 2013a] for two primary reasons. First, this study counts the total number (or frequency) of twice daily AR landfall detections while these previous papers identified the number of AR days. Second, data gap removal was handled differently here resulting in fewer identified data gaps in this study. AR days have previously been defined requiring landfalls in both IWV images in the twice daily data. This more restrictive definition was used in Neiman et al. [2008] and resulted in a mean of ~ 3 AR-days/month along the U.S. West Coast during the cool season. Wick et al. [2013a] required only one of the two IWV daily images to contain a landfalling AR to be considered an AR-day thus increasing the seasonal average to ~9 AR-days/month. Our approach using twice daily landfall data and updated gap definition results in about 40% more AR landfalls detected over the five year water year period (2004–2008) than those identified in Wick et al. [2013a].

4.2 Reanalysis ARs

4.2.1 AR frequency

Maps of the frequency of AR axis locations detected over the Pacific west of the U.S. West Coast, as is shown in Figure 2 for the satellite data, best displays the regions where ARs most likely originate and make landfall. The frequency of AR axis locations for the CFSR, MERRA, ERA-I, and 20CR data sets is shown in Figure 5, and their frequency patterns compare well with the satellite result shown in Figure 2, with maximum frequency in the southwestern portion of the domain and peak north of Hawaii. The highest AR frequencies extend northeastward toward the northern region of the U.S. West Coast. Among these three data sets, CFSR shows the highest frequency values and ERA-I shows the least. 20CR also peaks in the western part of the domain but has a more evenly distributed set of AR axis points along the AR corridor between

Hawaii and the U.S. Pacific Northwest. The magnitude of the AR frequencies in Figure 5 is significantly less for 20CR product (note scale change of 20CR color bar) at all grid cells, and the southeast part of the domain shows little or no AR detections. Fewer detections in the southeast region for all data sets has been shown in previous studies by Ralph et al. [2004] and Waliser et al. [2012] and may be influenced by the naturally shorter fetch with ARs extending from the tropics and exclusion of high IWV regions by the ARDT in the tropical reservoir. Furthermore, the reduced resolution of 20CR acts to both smooth IWV intensity and spatially broadens AR features such that some AR features may no longer meet the IWV intensity and AR width requirements in the AR definition.

A more direct method of comparing the reanalysis products with the satellite validation data is to construct the percentage of AR detections with respect to the satellite data at each grid cell. Figure 6 shows that CFSR, MERRA, and ERA-I all have a north to south gradient of detection percentages, with the reanalyses estimating fewer ARs in the northern part of the domain and more ARs in the southern part of the domain. ERA-I has the best agreement with satellite with mean absolute percentage difference of 20.6%, and CFSR shows the largest north-south gradient and more AR detections across the entire southern domain. The larger bias in CFSR may reflect the impact of no SSM/I radiance assimilation. However, MERRA and ERA-I also have a positive AR bias in the southeastern portion of the domain, concentrated near the Baja Peninsula. 20CR significantly underestimates AR detections relative to satellite at most latitudes but approaches 100% in the northeastern region off the coast of Washington. The north to south gradient for 20CR is the reverse of the other reanalyses data with the fewest AR detections in the southern portion of the domain due to less IWV in the southeastern domain (15^{o}N–25^{o}N,140^{o}W–110^{o}W).

4.2.2 AR landfall location

A comparison of the 15-year landfall statistics for each reanalysis product is compared to the satellite AR landfall climatology in Figure 7. The percentage of landfalls with respect to satellite shows CFSR, MERRA, and ERA-I with a slightly positive bias in AR landfalls, ranging from 103% to 105% of the satellite AR climatology. 20CR landfalls are shown for both the ensemble mean and median of ensemble members, with significantly fewer detected AR landfalls than satellite and the other reanalysis products. The median of ensembles has ~10% more AR landfalls than the ensemble mean. The red error bars for the ensemble mean give the minimum and maximum AR landfall percentage from the individual ensemble members. The ensemble mean landfall percentage remains outside of and below the spread of the ensemble members. Fewer AR landfalls in 20CR are due to fewer overall AR detections as was discussed in the previous section. These results also show that averaging the ensemble of IWV field acts to smooth out AR features enough to significantly reduce the number of detected landfalls. Finally, when CFSR is linearly interpolated from 0.5^{o} to 2.0^{o} (green bar, Figure 7), the percentage of AR detections decreases by ~20%; therefore, product resolution plays a significant role in AR identification, and likely contributes about half of 20CR's AR underestimation.

The seasonal and latitudinal variation of the 15-year AR landfall frequency for the satellite, CFSR, MERRA, ERA-I, 20CR ensemble mean, and 20CR median of ensembles show important differences between the reanalysis data sets. All of the data sets are shown in Figure 8 to have their maximum AR landfall frequency in October in the northern region of the U.S. West Coast between 45^{o}N and 50^{o}N. The high relative landfall frequencies in October and November agrees well between satellite and reanalysis data except for 20CR landfalls southward of 45^{o}N which has fewer landfall frequencies. Landfall frequencies decrease north of 42^{o}N after November but the decrease of landfall frequencies around 40^{o}N remains more steady until February. Frequencies are at a minimum in February but increase again around 40^{o}N in March. The 20CR increase of landfall frequencies in March appears further north than the other data. Differences between the 20CR ensemble mean and median of ensembles are generally higher values in all areas for the median data but particularly south of 45^{o}N.

In order to further identify AR landfall differences as function of latitude location, the 15-year AR landfall comparison was separated into two regions defined by the latitude of landfall. A northern region along the coast of Washington was defined to be 45^{o}N–50^{o}N and a southern region in southern California and Baja region was defined to be 30^{o}N–35^{o}N. AR detection percentages with respect to satellite AR climatology for these two regions are shown in Figure 9. AR landfalls in the northern region show better agreement across the four reanalyses than for the southern region. For the northern region, MERRA and CFSR are slightly under 100% and ERA-I is slightly above 100%. 20CR shows percentages of ~80% for the northern region, significantly higher than the ~50% shown for the entire U.S. West Coast. The southern region shows larger differences across all four reanalyses and greater differences with the satellite climatology. ERA-I best agrees with satellite AR landfalls in the southern region with a percentage near 100%. The ARDT identified ~20% more AR landfalls for MERRA and CFSR than satellite, and the AR detection percentage for 20CR was smaller than other reanalyses with 29.3% for the ensemble mean and 55.0% for the median of the ensembles (25.7% difference). This difference contrasts with the northern region where the 20CR ensemble mean and median AR percentages had difference of only 3.5%. The ensemble spread for the southern region is 6.6% larger than the northern region indicating more uncertainty with detecting AR landfalls for the southern region.

4.2.3 AR landfall characteristics

AR landfall characteristics including IWV core, minimum width, directional angle, and landfall latitude biases were examined among the four reanalysis products and the satellite data and results are provided in Table 2. The satellite mean data for these characteristics compared well with previous results from Wick et al. [2013b] and was in good agreement with the reanalysis data sets. The core IWV values for landfalling ARs were drier for the reanalysis data but had less than 0.1 cm difference with the satellite data for CFSR, MERRA, and ERA-I. The 20CR ensemble mean had the largest dry bias of 0.21 cm. Small minimum width differences occur between satellite and CFSR, MERRA, and ERA-I, but 20CR shows a 63 km wider AR landfall width due to the lower resolution of that product. Directional angle for all reanalysis products has landfalling ARs oriented about 4 to 11 degrees more northward at landfall than satellite data with 20CR closest to satellite results and ERA-I having the largest angle difference. However, this slightly more northward directional angle is likely within the uncertainty of the technique used to determine this angle. Landfall latitude bias was less than 100 km for all reanalysis products indicating good agreement on landfall position. A latitude landfall bias for all reanalysis products indicated a northerly bias which is most likely due to a ~ 2 hour delay in the satellite observation time with the reanalysis output time.

4.2.4 Simultaneous AR landfall occurrence

The ability for the reanalysis data sets to represent the satellite observations of AR landfalls was tested using traditional statistical measures of probability of detection (POD) and false alarm rate (FAR). The POD is defined as the fraction of cases where a satellite AR landfall was accurately represented in a reanalysis product. The FAR is the fraction of reanalysis AR landfalls that did not occur in the satellite observations. An AR landfall match between reanalysis and satellite was deemed to occur if AR landfall occurred on the same day and within 3^{o} latitude of each other. This condition was applied to ensure detection statistics were based on matched AR landfalls. Statistics were derived over the 15-year record of the data sets. 20CR data results are only from the ensemble mean data.

The monthly climatology of POD statistics for each reanalysis product are shown in Figure 10a. POD is highest in the first two months of the cool season for all four data sets and a downward trend occurs through February with March showing higher POD for all but the 20CR data. CFSR AR POD was the highest over the 15-year period. MERRA and ERA-I AR POD are less than CFSR by no more than 0.06, whereas 20CR had the lowest POD among the four data sets. MERRA is impacted by the 3^{o} latitude restriction and compares well with CFSR and ERA-I when this condition is removed as is shown with landfall latitude bias in Table 2. However, MERRA AR landfall locations have less agreement with the satellite AR data when using the 3^{o} latitude requirement. 20CR POD results are impacted by the significantly fewer AR detections along the southern region of the U.S. West Coast. POD results are generally better in the early season due to better agreement for north U.S. West Coast AR landfalls among all the data sets. The FAR (Figure 10b) also shows a downward trend throughout the cool season for all four data sets. The highest FAR values occur during the early cool season during more frequent AR landfalls, in particular along the northern region of the U.S. West Coast. The 15-year FAR is highest for MERRA due to mismatched AR locations as noted previously but CFSR and ERA-I have a similar result. 20CR's underestimation of the number of AR landfalls results in it having the fewest falsely detected AR landfalls.

Previous estimates of POD and FAR for AR landfalls within numerical weather prediction (NWP) models over three cool seasons were calculated in Wick et al. [2013b]. POD of AR landfalls at the analysis time for these models generally ranged from 0.75 to 0.9 which is higher than shown here. This difference can be explained by our imposed 3^{o} latitude restriction: When this restriction is removed the POD results for CFSR, ERA-I, and MERRA increase to between 0.8 and 0.9. FAR results for AR landfalls in Wick et al. [2013b] range from 0.2 to 0.3 which is significantly higher than with the reanalysis products shown here. The POD also trends to slightly higher values from 1998 to 2012 for CFSR, ERA-I, and MERRA (not shown). This is likely due to more satellite observations included in these reanalysis products at the end of the time period.

5. CONCLUSIONS

An assessment of AR landfall frequency for the U.S. West Coast for the cool season over a 15-year period from October 1997 to March 2012 was conducted using SSM/I and SSMIS satellite observations and four reanalysis data sets. While interannual AR landfall frequency varies greatly, gaps in satellite observations also impact the data sampling and likely impact this variability. The percentage of twice daily satellite AR detections over a cool season varies from 27%–45%. The frequency in AR detection is higher than previous studies, due in part to fewer gaps removed from the satellite observations in this study. The monthly climatology using the ARDT method has the highest AR landfall percentage and frequency in October and the lowest in February in agreement with previous studies.

AR U.S. West Coast landfall frequency is generally well characterized in the CFSR, MERRA, and ERA-I reanalysis data sets as compared to satellite observations. The 15-year percentage of AR landfalls in these three reanalyses with respect to satellite ranges from 103% to 105%. All three reanalyses had their highest AR landfalls occur in the northern region in October. ERA-I AR landfall percentages were slightly greater than 100% for both the northern and southern region and showed the most consistent AR landfall percentage while MERRA and CFSR had slightly less than 100% for the northern region but upwards of 120% for the southern region. AR frequency maps also show the lowest AR detection error rate between satellite and ERA-I. CFSR shows significantly more AR detections south of 25^{o}N than the other three reanalyses. This larger difference is likely due to the greater degree of independence from the satellite data in CFSR since SSM/I radiances were not assimilated while MERRA and ERA-I did assimilate SSM/I radiances.

Significantly fewer AR landfalls were identified in 20CR due to several factors. One factor is the lower spatial resolution of the 20CR product reduces the number of AR landfall detections. Interpolating CFSR data to the 20CR data resolution reduced the AR landfall percentage by 20%, suggesting that about half of 20CR's underestimation is due to its coarse resolution; the ARDT likely has greater uncertainty in detecting AR features from lower resolution data. 20CR ensemble mean data was found to have ~10% fewer AR landfall detections than the median of the ensemble members. Both of these factors act to smooth narrow and marginally weak ARs such that they are no longer detectable with ARDT. A third factor is notably fewer AR landfalls in the southern region of the U.S. West Coast for 20CR. While AR landfall percentages for 20CR for the northern region of the U.S. West Coast compare well with satellite and other reanalysis products, the southern region had significantly fewer AR landfalls, particularly for the 20CR ensemble mean data which had 25% fewer landfalls than the median result.

Statistical measures of probability of detections (POD) and false alarm rate (FAR) of AR landfalls show the highest POD for CFSR of 0.73. Even though satellite and reanalysis agreed well in the total frequency of AR landfalls, a little more than one quarter of landfalls in reanalysis did not match with satellite. POD and FAR monthly climatologies show highest values in October and November and lowest values in February and March. 15-year FAR is highest for MERRA at 15% but only 1–2% points higher than CFSR and ERA-I. Because of fewer AR landfall detections, 20CR had both the lowest POD and FAR. POD and FAR rates are less than previously reported using AR landfalls detected in NWP models, likely due to a more restrictive definition of a matched AR between reanalysis and satellite data.

This analysis provides insight and confidence for using reanalysis products for AR landfall detections along the U.S. West Coast. Reanalysis products have the advantage over satellite data of having complete time and space sampling and generally longer time records, but have greater uncertainty for earlier time periods where few observations are assimilated. From these reanalysis data, AR landfall climatologies can be developed and compared with other indices of atmospheric and oceanic variability that may impact the subseasonal-to-decadal variability of AR landfalls on the U.S. West Coast. Also with reanalysis data, a further step could be taken to identify AR landfalls using integrated vapor transport (IVT) which is more direct measure of water vapor flux along an AR. Such climatologies should prove useful in better understanding U.S. West Coast extreme precipitation events and their possible relationship with seasonal (MJO) and interannual (ENSO) variability.

ACKNOWLEDGMENTS

This study was supported by NOAA Climate Observations and Monitoring Program # NOAA-OAR-CPO-2012-2003041. We would like to thank three anonymous reviewers who provided insightful comments that improved this paper. ERA-I, CFSR, and 20CR data was provided by the NOAA-ESRL Physical Sciences Division, Boulder Colorado from their web site at http:/www.esrl.noaa.gov/psd. MERRA data were acquired from the Goddard Earth Sciences (GES) Data and Information Center (DISC). Satellite data were acquired from the NOAA Comprehensive Large Array-Data Stewardship System (CLASS).

6. REFERENCES

Compo G.P. and Co-Authors (2011), Review article the Twentieth Century Reanalysis Project, *Q.J.R. Meteorol. Soc.*, *137*, 1-28.

Dee, D.P., and Co-Authors (2011), The ERA-Interim reanalysis: configuration and performance of the data assimilation system, *Q.J.R. Meteorol. Soc.*, *137*, 553–597.

Dettinger, M.D., F.M. Ralph, T. Das, P.J. Neimann, and D. Cayan (2011), Atmospheric rivers, floods, and the water resources of California, *Water*, *3*, 455–478.

Hughes, M., K.M. Mahoney, P.J. Neiman, B.J. Moore, M. Alexander, F.M. Ralph (2014), The Landfall and Inland Penetration of a Flood-Producing Atmospheric River in Arizona. Part II: Sensitivity of Modeled Precipitation to Terrain Height and Atmospheric River Orientation. *J. Hydrometeor.*, *15*, 1954–1974.

Lavers, D.A., G. Valarini, R.P. Allan, E.F. Wood, and A.J. Wade (2012), The detection of atmospheric rivers in atmospheric reanalyses and their links to British winter floods and the large-scale climatic circulation, *J. Geophys. Res.*, *117*, doi:10.1029/2012JD018027.

Lavers D.A., and G. Villarini (2013), The nexus between atmospheric rivers and extreme precipitation across Europe, *Geophys. Res. Lett.*, *40*, 3259–3264, doi:10.1002/grl50636.

Neiman, P.J., F.M. Ralph, G.A. Wick, J.D. Lunquist, and M.D. Dettinger (2008), Meteorological characteristics and overland precipitation impacts of atmospheric rivers affecting the west coast of North America based on eight years of SSM/I satellite observations, *J. Hydrometeor.*, *9*, 22–47.

Neiman, P.J., L.J. Schick, F.M. Ralph, M. Hughes, and G.A. Wick (2011), Flooding in western Washington: The connection to atmospheric rivers, *J. Hydrometeor*., *12*, 1337–1358.

Payne A.E., and G. Magnusdottir (2014), Dynamics of landfalling atmospheric rivers over the north pacific in 30 years of MERRA reanalysis, *J. Clim*, 27, 7133–7150, doi:10.1175/JCLI-D-14-00034.1

Rayner, N.A., D.E. Parker, E.B. Horton, C.K. Folland, L.V. Alexander, D.P. Rowell, E.C. Kent, A. Kaplan (2003), Global analyses of sea surface temperature, sea ice, night marine air temperature since the late nineteenth century, *J. Geophys. Res*., *108(D14)*, 4407, doi:10.1029/2002JD002670.

Ralph, F.M., P.J. Neiman, and G.A. Wick (2004), Satellite and CALJET aircraft observations of atmospheric rivers over the eastern North Pacific Ocean during the winter of 1997/98, *Mon. Wea. Rev*., *132*, 1721–1745.

Ralph, F.M., P.J. Neiman, G.N. Kiladis, K. Weickmann, and D.W. Reynolds (2011), A multiscale observational case study of a pacific atmospheric river exhibiting tropical-extratropical connections and a mesoscale frontal wave, *Mon. Wea. Rev*., *139*, 1169–1189, doi:10.1175/2010MWR3596.1.

Ralph, F.M., and M.D. Dettinger (2012), Historical and national perspectives on extreme West Coast precipitation associated with atmospheric rivers during December 2010, *Bull. Amer. Meteor. Soc*., *93*, 783–790.

Rayner N.A., D.E. Parker, E.B. Horton, C.K. Folland, L.V. Alexander, D.P. Rowell, E.C. Kent, and A. Kaplan (2003), Global analyses of sea surface temperature, sea ice, and night marine air temperature since the late nineteenth century, *J. Geophys. Res.*, *108*, doi:1029/2002JD002670.

Rienecker M.M. and Co-Authors (2011), MERRA: NASA's modern-era retrospective analysis for research and applications, *J. Climate*, *24*, 3624–3648, doi:10.1175/JCLI-D-11-00015.1.

Rutz, J.J., W.J. Steenburgh, and F.M. Ralph (2014), Climatological characteristics of atmospheric rivers and their inland penetration over the western united states, *Mon. Wea. Rev.*, *142*, 905–921, doi:http://dx.doi.org/10.1175/MWR-D-13-00168.1.

Ryoo, J.-M., Y. Kaspi, D.W. Waugh, G.N. Kiladis, D.E. Waliser, E.J. Fetzer, and J. Kim (2013), Impact of rossby wave breaking on U.S. west coast winter precipitation during ENSO events, *J. Clim*, 26, 6360–6382, DOI:10.1175/JCLI-D-12-00297.1.

Saha, S. and Co-Authors (2010), The NCEP climate forecast system reanalysis, *Bull. Amer. Meteor. Soc.*, *91*, 1015–1057, doi:10.1175/2010BAMS3001.1.

Waliser, D. E and Co-Authors (2012), The year of tropical convection (May 2008–April 2010): climate variability and weather highlights. *Bull. Amer. Meteor. Soc*. *93*, 1189–1218. doi: 10.1175/2011BAMS3095.1

Wentz, F.J. (1995), The intercomparison of 53 SSM/I water vapor algorithms. Remote Sensing Systems Tech. Rep. on the WetNet Water Vapor Intercomparison Project (VIP), Remote Sensing Systems, Santa Rosa, CA, 19pp.

Wick. G.A., P.J. Neiman, and F.M. Ralph (2013a), Description and validation of an automated objective technique for identification and characterization of the integrated water vapor signature of atmospheric rivers, *IEEE Trans. Geosci. Remote Sens*., *51*, 2166–2176, doi10.1109/TGRS2012.2211024.

Wick, G.A., P.J. Neiman, F. M. Ralph, and T.H. Hamill (2013b), Evaluation of forecasts of the the water vapor signature of atmospheric rivers in operational numerical weather prediction models, *Wea. Forecasting*, *28*, 1337–1352, doi:10.1175/WAF-D-13-00025.1.

Zhu, Y., and R.E. Newell (1998), A proposed algorithm for moisture fluxes from atmospheric rivers, *Mon. Wea. Rev*., *126*, 725–735.

7. TABLES

Table 1: Summary of time and spatial characteristics of reanalysis data sets.

Product	Time period (years)	Product spatial resolution (longitude x latitude) in degrees	Product time resolution (UTC)
CFSR	1979–present	0.5^{o} x 0.5^{o}	0000,0600,1200,1800
MERRA	1979–present	0.67^{o} x 0.5^{o}	0000,0600,1200,1800
ERA-I	1989–present	0.7^{o} x 0.7^{o}	0000,0600,1200,1800
20CR	1871–present	2.0^{o} x 2.0^{o}	0000,0600,1200,1800

Table 2: Satellite 15-year cool season mean and bias (reanalysis-satellite) in IWV, AR width, angle, and landfall latitude statistics conditioned on both satellite and reanalysis AR landfall. 20CR_MN is derived from the ensemble mean data, 20CR_MD is the median of the ensemble member data, and 20CR_SPD is the spread of the ensemble members from minimum to maximum.

	Satellite Mean	MERRA Bias	ERA-I Bias	CFSR Bias	20CR_MN Bias	20CR_MD Bias	20CR_SPD	
							Max	Min
IWV (cm)	2.71	-0.02	-0.06	-0.09	-0.21	-0.18	-0.16	-0.21
Width (km)	261.7	-6.5	-12.4	-5.3	63.1	63.4	68.3	56.7
Angle (degrees)	47.3	-5.6	-11.2	-8.0	-3.9	-5.6	-3.4	-8.4
Landfall Latitude (degrees)	41.4	0.37	0.72	0.23	0.87	0.77	0.90	0.58

8. FIGURE CAPTIONS

Figure 1: Example of AR for March 27, 2005 depicted with IWV fields from satellite observations from SSM/I and CFSR, 20CR, MERRA, and ERA-I reanalysis data sets. Grey dots indicate axis locations determined by ARDT as the center axis locations of the AR. 20CR IWV data is from the ensemble mean data set.

Figure 2: A map of the frequency of AR axis locations detected by ARDT using 1.0 degree grid spacing for twice daily satellite observations from SSM/I and SSMIS data for 15 cool seasons (October–March) for water years 1998–2012.

Figure 3: (a) Time series of the frequency (blue) of AR landfalls detected by ARDT using 0.5 degree SSM/I and SSMIS IWV data for the cool season for water years 1998–2012. Frequency based on twice daily satellite IWV imagery. Time series of percentage of AR landfalls (green) for the same time period is also shown. (b) Time series of the number of occurrences where gaps in the SSM/I and SSMIS data prevented ARDT from performing detection for a given IWV image. Annual maximum occurrences for a non-leap year during the cool season is 364.

Figure 4: Monthly climatology of AR landfall frequency and percentage along the U.S. West Coast (31^{o}N–50^{o}N) derived from SSM/I and SSMIS IWV data for 15 cool seasons for water years 1998–2012.

Figure 5: A map of AR axis location frequency using (a) CFSR, (b) MERRA, (c) ERA-I, and (d) 20CR IWV data for water years 1998–2012. Note change in color bar scale for 20CR (maximum = 600) differs from the other three figures (maximum = 1800).

Figure 6: Maps of AR axis percentage relative to satellite for (a) CFSR, (b) MERRA, (c) ERA-I, and (d) 20CR for water years 1998–2012. Mean absolute percentage difference given in parenthesis. Note that 20CR color bar maximum is 100 which is half of the maximum value for the other three figures.

Figure 7: Percentage of AR landfalls relative to satellite for water years 1998–2012 for MERRA, ERA-I, CFSR, 20CR ensemble mean (20CR_MN), and 20CR median of ensembles (20CR_MD). Green bar indicates CFSR result using 2.0^{o} IWV data rather than 0.5^{o} used for all other data in this bar plot. Red indicates maximum and minimum percentages for the 56 ensemble members of 20CR.

Figure 8: Total AR landfall frequency for each month in 1^{o} latitude bins over the 15-year period.

Figure 9: Percentage of reanalysis AR landfalls relative to satellite for water years 1998–2012 for MERRA, ERA-I, CFSR, 20CR ensemble mean (20CR_MN), and 20CR median of ensembles (20CR_MD). Blue bar indicates AR landfall percentage for 45^{o}N–50^{o}N and green bar indicates

AR landfall percentage for 30^{o}N–35^{o}N. Light blue indicates 20CR ensemble spread and dark line in middle of light blue indicates median.

Figure 10: (a) The probability of detection (POD) and (b) the false alarm rate of AR landfalls for water years 1998–2012 as a function of month. AR match required AR landfall to occur on the same day and within 3^{o} of latitude. 15-year mean POD and FAR values given in legend.

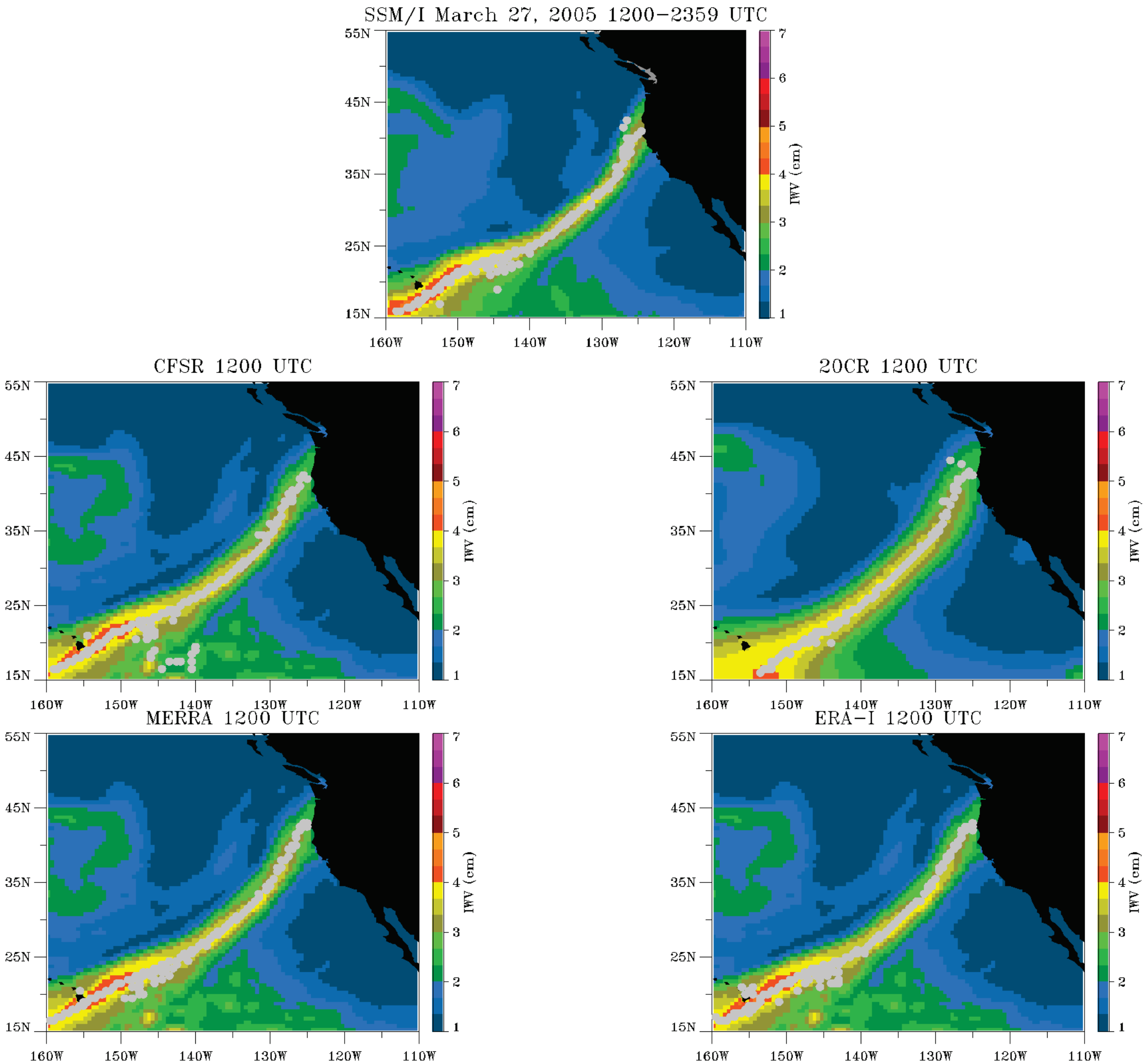

Figure 1: Example of AR for March 27, 2005 depicted with IWV fields from satellite observations from SSM/I and CFSR, 20CR, MERRA, and ERA-I reanalysis data sets. Grey dots indicate axis locations determined by ARDT as the center axis locations of the AR. 20CR IWV data is from the ensemble mean data set.

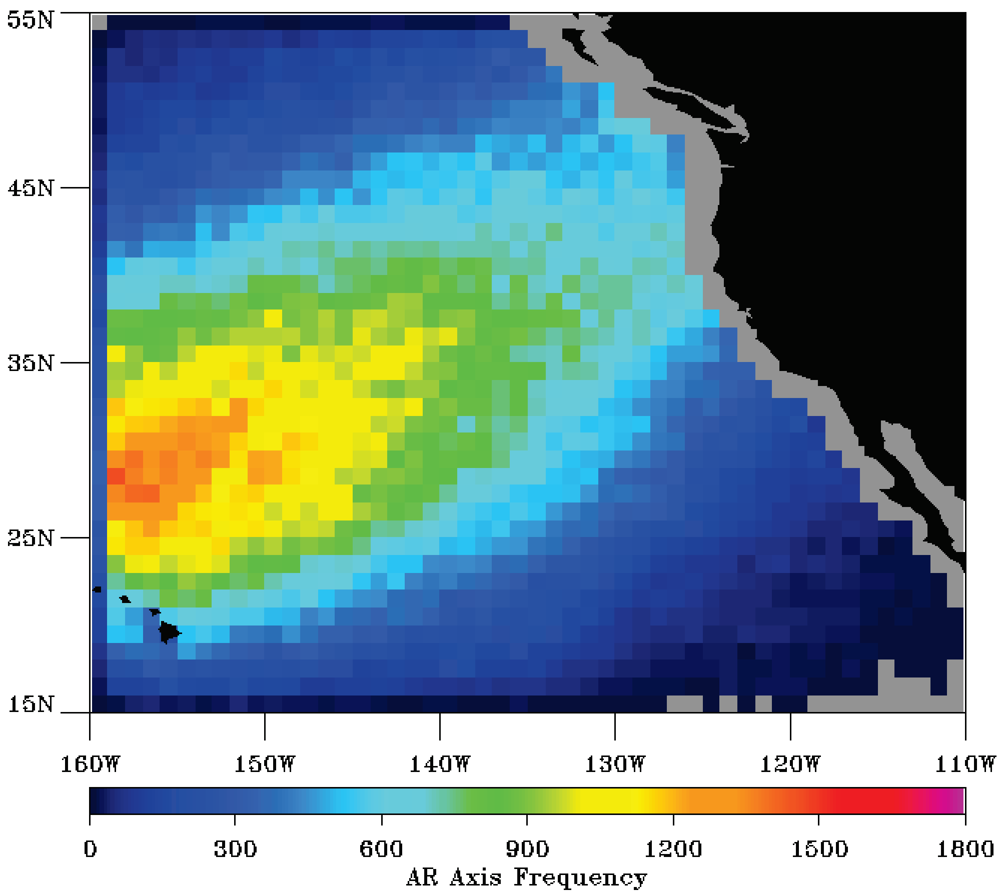

Figure 2: A map of the frequency of AR axis locations detected by ARDT using 1.0 degree grid spacing for twice daily satellite observations from SSM/I and SSMIS data for 15 cool seasons (October–March) for water years 1998–2012.

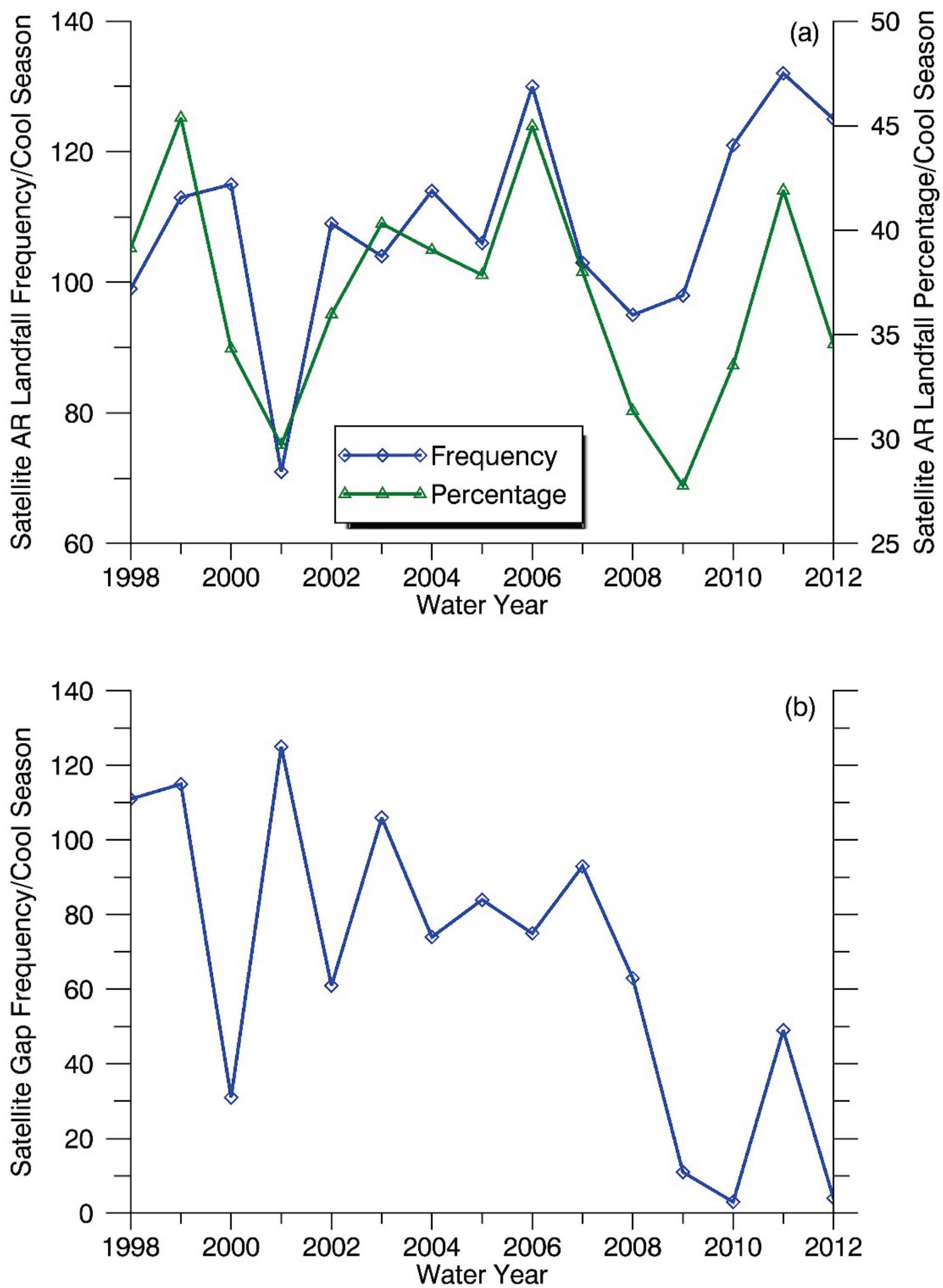

Figure 3: (a) Time series of the frequency (blue) of AR landfalls detected by ARDT using 0.5 degree SSM/I and SSMIS IWV data for the cool season for water years 1998–2012. Frequency based on twice daily satellite IWV imagery. Time series of percentage of AR landfalls (green) for the same time period is also shown. (b) Time series of the number of occurrences where gaps in the SSM/I and SSMIS data prevented ARDT from performing detection for a given IWV image. Annual maximum occurrences for a non-leap year during the cool season is 364.

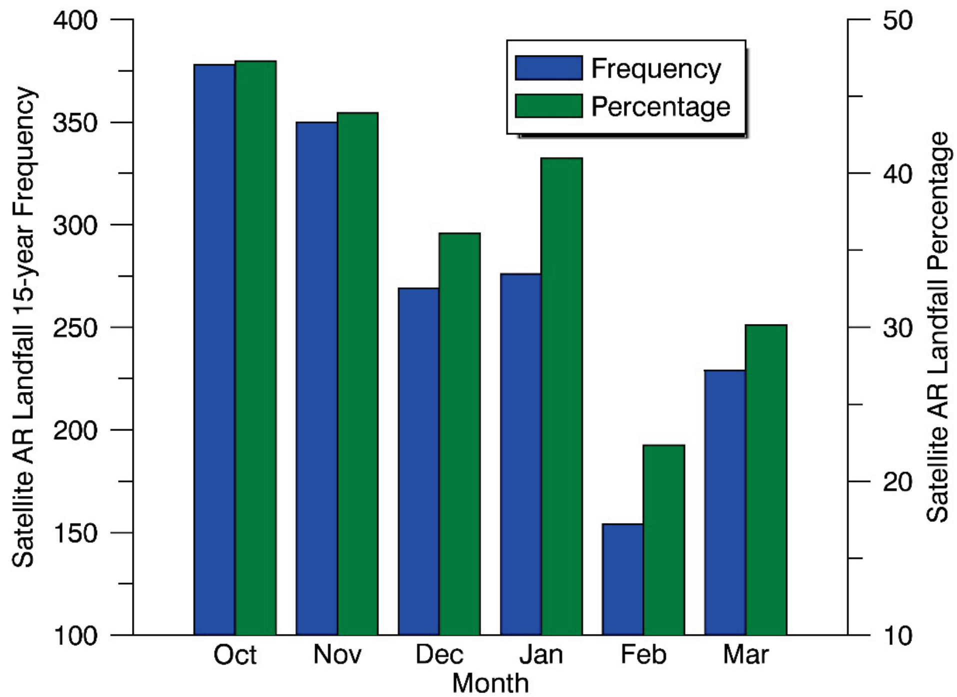

Figure 4: Monthly climatology of AR landfall frequency and percentage along the U.S. West Coast (31^{o}N–50^{o}N) derived from SSM/I and SSMIS IWV data for 15 cool seasons for water years 1998–2012.

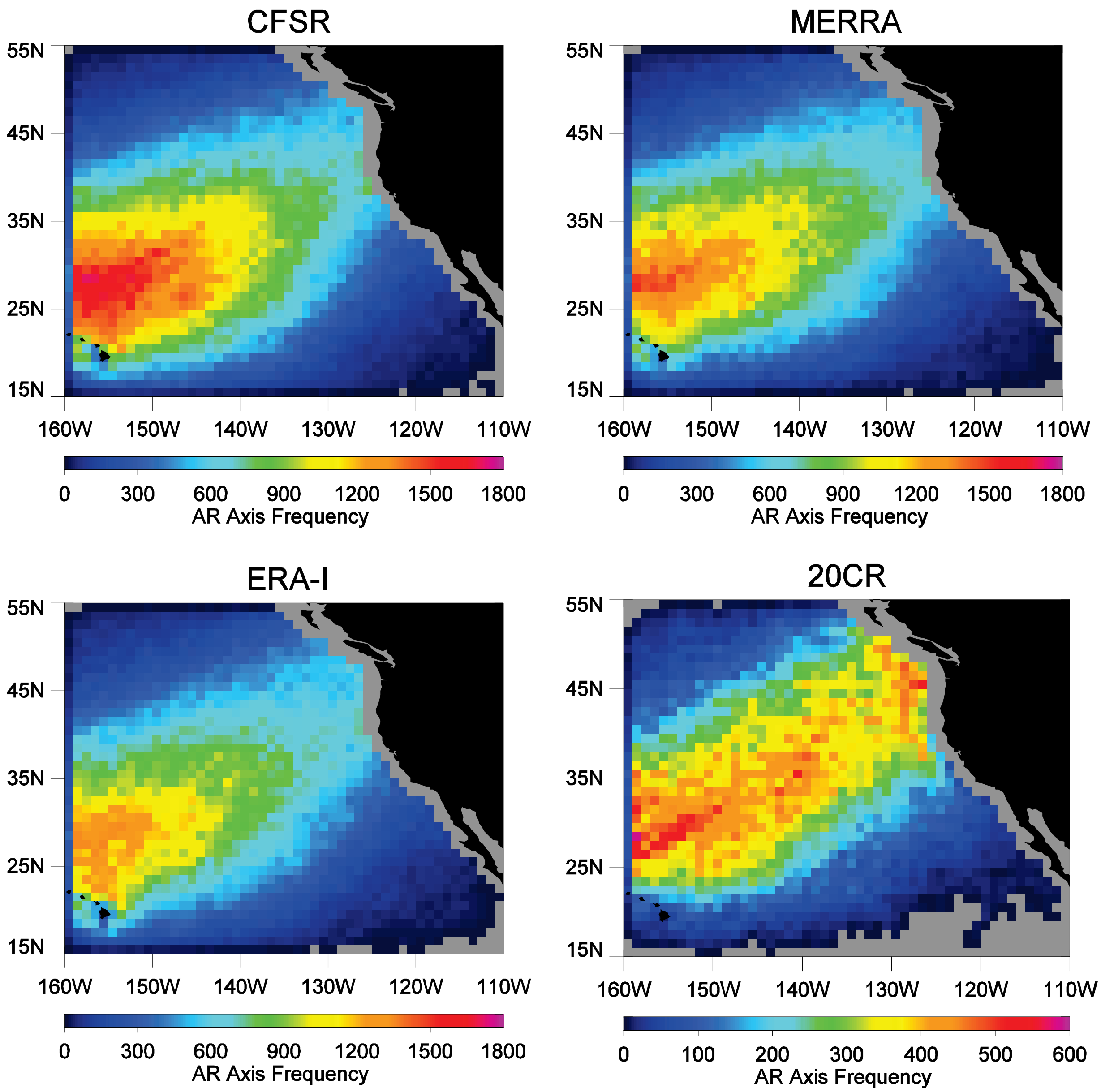

Figure 5: A map of AR axis location frequency using (a) CFSR, (b) MERRA, (c) ERA-I, and (d) 20CR IWV data for water years 1998–2012. Note change in color bar scale for 20CR (maximum = 600) differs from the other three figures (maximum = 1800).

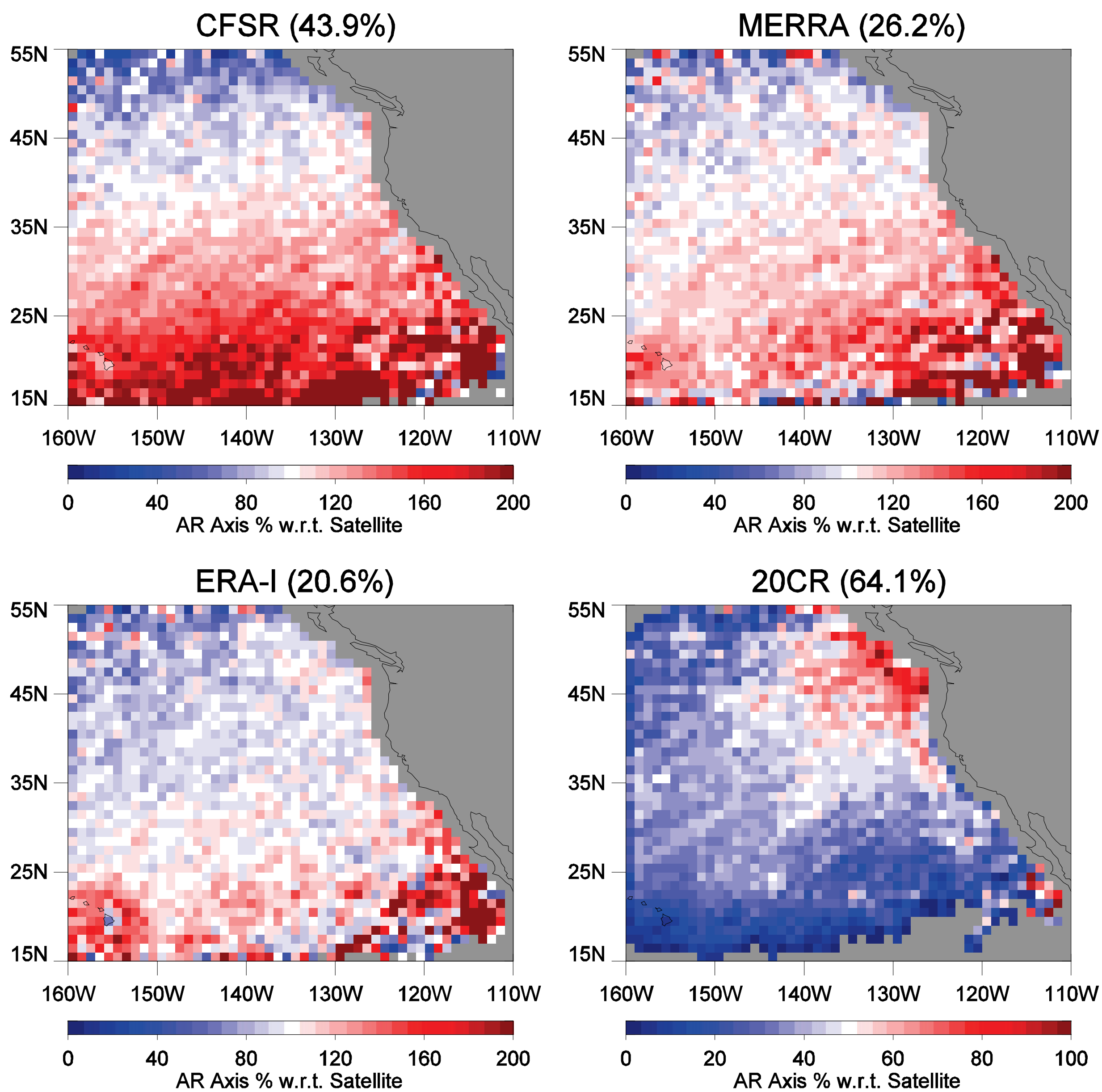

Figure 6: Maps of AR axis percentage relative to satellite for (a) CFSR, (b) MERRA, (c) ERA-I, and (d) 20CR for water years 1998–2012. Mean absolute percentage difference given in parenthesis. Note that 20CR color bar maximum is 100 which is half of the maximum value for the other three figures.

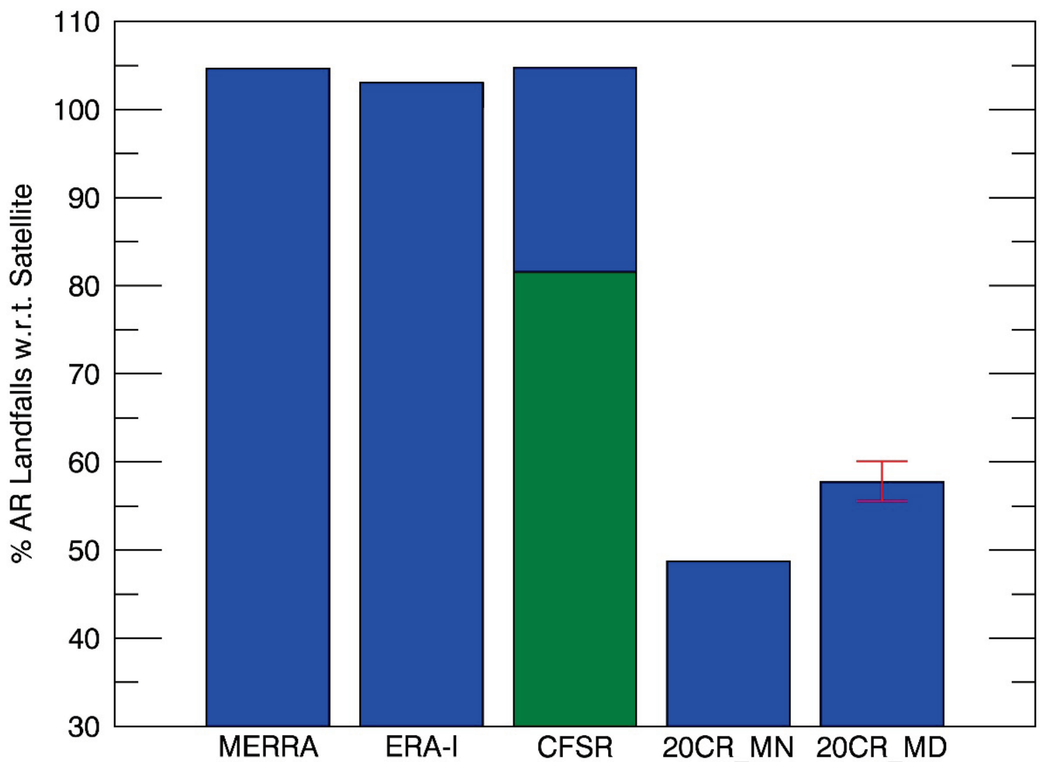

Figure 7: Percentage of AR landfalls relative to satellite for water years 1998–2012 for MERRA, ERA-I, CFSR, 20CR ensemble mean (20CR_MN), and 20CR median of ensembles (20CR_MD). Green bar indicates CFSR result using 2.0^o IWV data rather than 0.5^o used for all other data in this bar plot. Red indicates maximum and minimum percentages for the 56 ensemble members of 20CR.

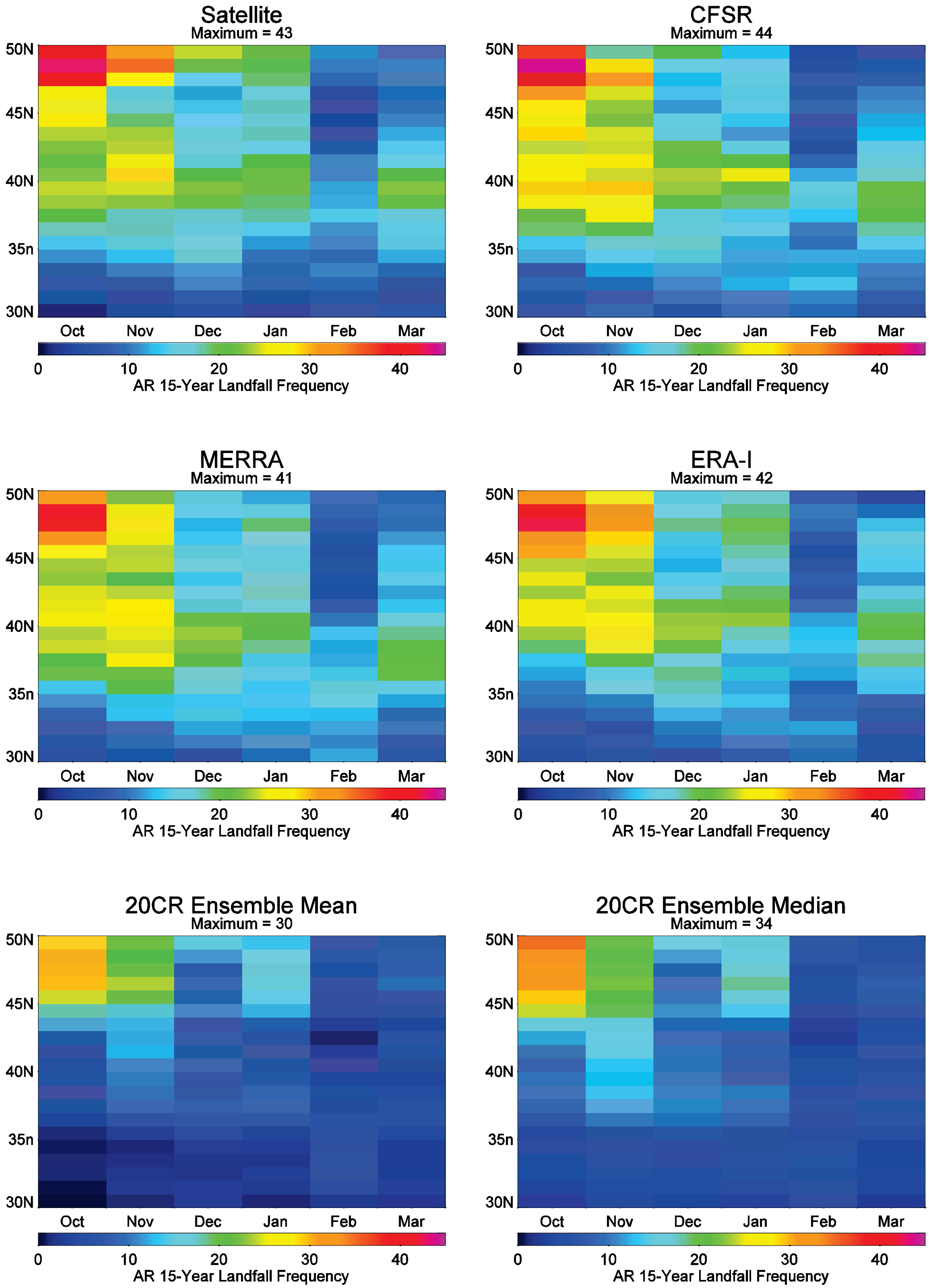

Figure 8: Total AR landfall frequency for each month in 1° latitude bins over the 15-year period.

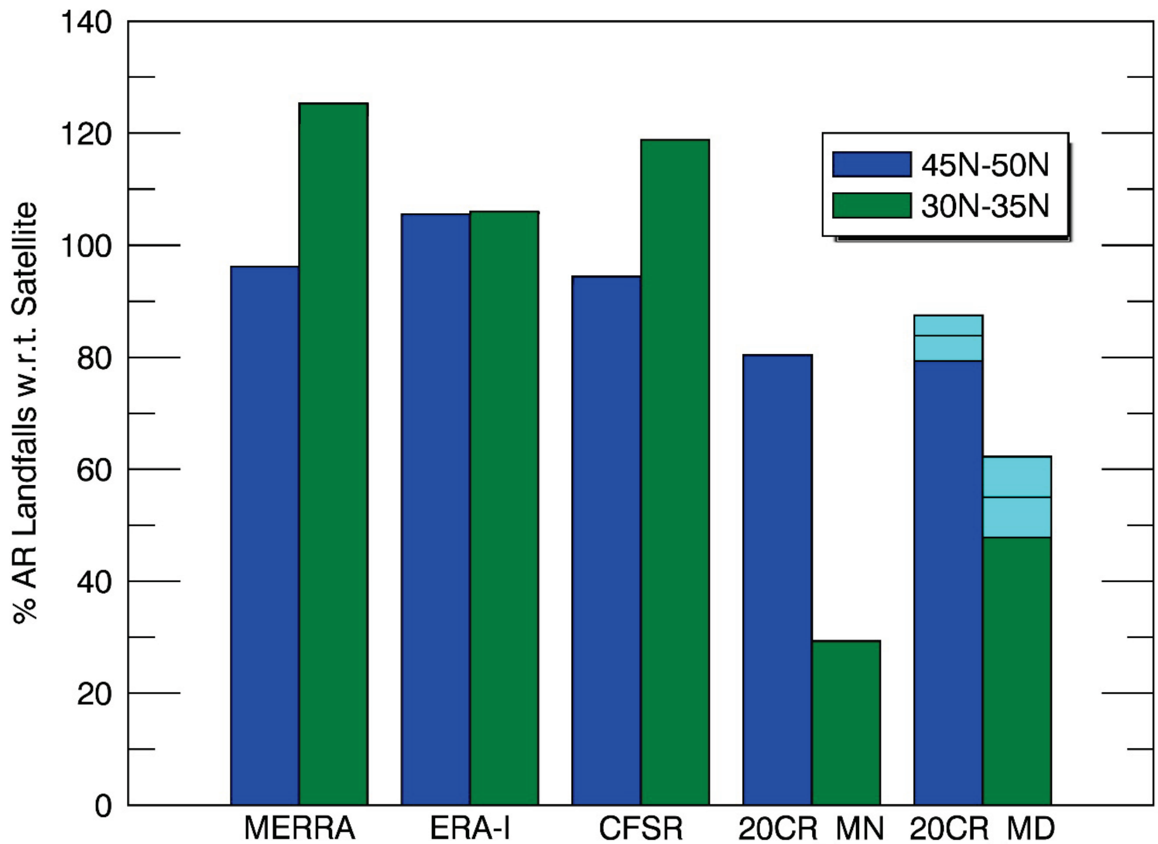

Figure 9: Percentage of reanalysis AR landfalls relative to satellite for water years 1998–2012 for MERRA, ERA-I, CFSR, 20CR ensemble mean (20CR_MN), and 20CR median of ensembles (20CR_MD). Blue bar indicates AR landfall percentage for 45^{o}N–50^{o}N and green bar indicates AR landfall percentage for 30^{o}N–35^{o}N. Light blue indicates 20CR ensemble spread and dark line in middle of light blue indicates median.

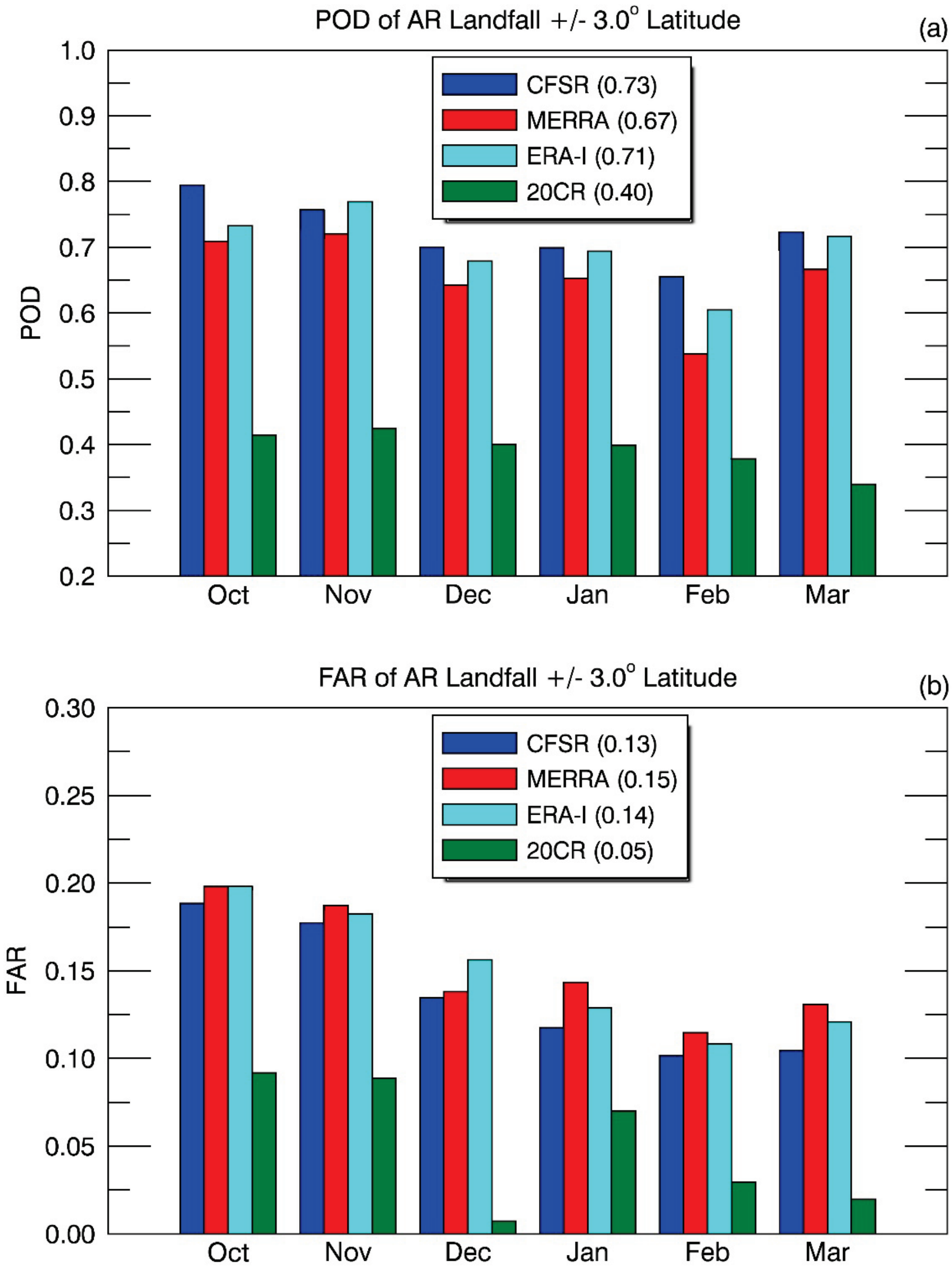

Figure 10: (a) The probability of detection (POD) and (b) the false alarm rate of AR landfalls for water years 1998–2012 as a function of month. AR match required AR landfall to occur on the same day and within 3^o of latitude. 15-year mean POD and FAR values given in legend.